The Journal of Experimental Biology 199, 2253–2268 (1996)
Printed in Great Britain © The Company of Biologists Limited 1996
JEB0451

HETEROCERCAL TAIL FUNCTION IN LEOPARD SHARKS: A THREE-DIMENSIONAL KINEMATIC ANALYSIS OF TWO MODELS

LARA A. FERRY AND GEORGE V. LAUDER*

Department of Ecology and Evolutionary Biology, University of California at Irvine, Irvine, CA 92697-2525, USA

Accepted 1 July 1996

Summary

Two different models have been proposed to explain the function of the heterocercal tail in shark locomotion. The classical model proposes that, as a result of lift generated by the tail as it beats, the net force acting on the tail is directed dorsally and anteriorly. In contrast, Thomson's model suggests that the tail generates a net force directed through the shark's center of gravity, i.e. ventrally and anteriorly. In this study, we evaluate these two models by describing the three-dimensional kinematics of the heterocercal tail in the leopard shark *Triakis semifasciata* during swimming. Lateral and posterior views of the tail were examined from four individuals swimming in a flow tank at 1.2 L s^{-1} (where L is total length) using two high-speed video cameras filming simultaneously at 250 fields s^{-1}. These two simultaneous views allowed eight landmarks on the tail to be followed in three dimensions through time. These landmarks allowed the tail to be divided into separate surfaces whose orientation over time was calculated. Points located anteriorly on the tail go through significantly smaller excursions and reach their maximum lateral excursion significantly earlier in the beat cycle than points on the trailing edge of the tail. Three-dimensional angle calculations show that the terminal lobe leads the ventral lobe through a beat, as predicted by the classical model. Dye-stream visualizations confirmed that this pattern of movement deflects water ventrally and posteriorly to the moving tail, providing strong support for the classical model. Additionally, our results show that a three-dimensional analysis is critical to understanding the function of the heterocercal tail.

Key words: leopard shark, *Triakis semifasciata*, swimming, locomotion, kinematics, tail function.

Introduction

The tail of fishes has attracted the attention of numerous hydrodynamicists and morphologists interested in locomotor structure and function (e.g., Affleck, 1950; Alexander, 1965; Webb, 1973, 1975; Videler, 1975; Thomson and Simanek, 1977; Webb and Smith, 1980; Lauder, 1989). Tail shape in the most diverse clade of fishes, the Teleostei, is generally characterized as homocercal or having symmetrical external structure (the dorsal and ventral lobes are similar in size and shape). In contrast, the tail of many sharks, primitive ray-finned fishes and early fossil vertebrates is asymmetrical in external shape. In this heterocercal tail, the vertebral column extends into the upper (terminal) lobe. Heterocercal tail shape is generally considered to be primitive for gnathostomes, although early vertebrates possess tails with many different shapes (Olson, 1971; Hopson, 1974; Webb and Smith, 1980; Carroll, 1988; Wilson and Soehn, 1990).

The most diverse extant clade of fishes with well-developed heterocercal tails is the Elasmobranchiomorphi (sharks and their relatives), and the morphology and function of the heterocercal tail in sharks has been the focus of several studies (e.g. Alexander, 1965; Simons, 1970; Reif and Weishampel, 1986; Keithan *et al.* 1992). A fundamental disagreement has arisen over the functional consequences of heterocercal tail shape. While the homocercal tail with its equally sized dorsal and ventral lobes might be expected to generate force directed only anteriorly (Gosline, 1971), the functional consequences of the morphologically asymmetrical heterocercal shark tail are less clear (Aleev, 1969). Currently, there are two different models of heterocercal tail function.

The first model has been contributed to by many authors (see Grove and Newell, 1936; Affleck, 1950; Bainbridge, 1963; Alexander, 1965; Aleev, 1969; Simons, 1970) and we will refer to it as the classical model (Fig. 1). In the classical model of heterocercal tail function, the dorsal edge of the tail is believed to be relatively stiff (owing to support by the vertebral column) and, therefore, should lead the ventral region of the tail as it beats from side to side (Alexander, 1965; Simons, 1970; Olson, 1971). As a result of the smaller (ventral) lobe lagging behind the stiffer dorsal tail edge, the caudal fin moves through the water at an angle to the horizontal, thus generating a lift force (Fig. 1, posterior view). Both Alexander (1965) and Simons (1970) performed experiments using the severed tails

*Author for correspondence (e-mail: glauder@uci.edu).

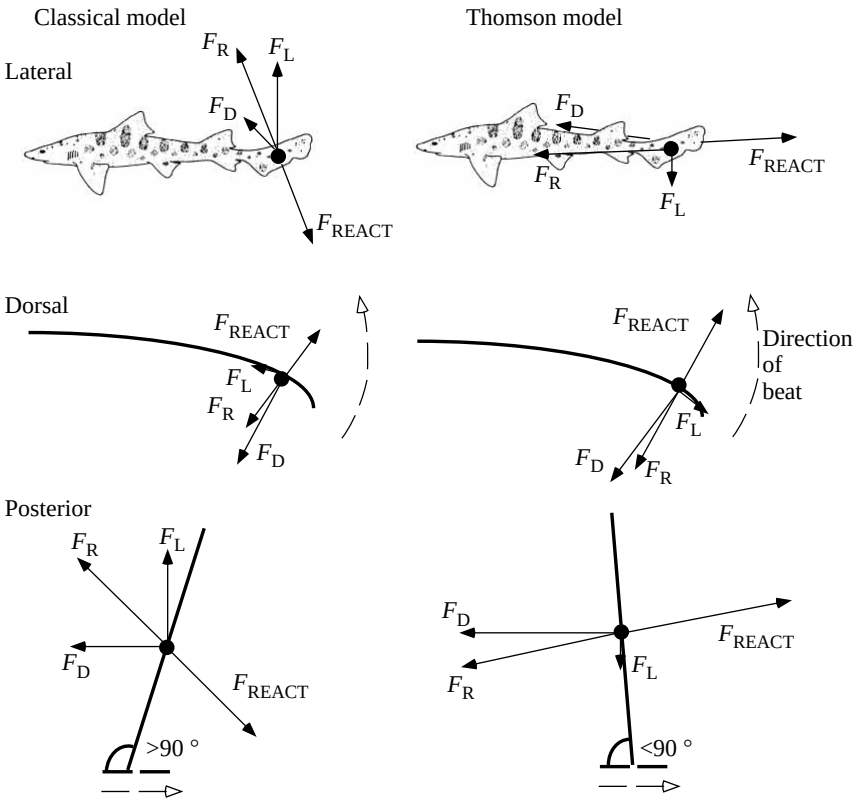

Fig. 1. Schematic summaries of two models (classical and Thomson) depicting the forces acting on the shark tail during locomotion from three views: lateral, dorsal and posterior. The key feature of the classical model of heterocercal tail function is that the tail produces a lift force (F_L) that generates a torque about the center of mass. This torque is countered by an equal and opposite torque generated by lift forces at the pectoral fins. The net lift force on the shark is balanced by gravity acting on the shark's negatively buoyant mass. Movement of the tail also results in a drag force that is generated in the direction opposite to the tail's movement and perpendicular to the lift generated (F_D). These lift and drag force vectors can be summed to produce a resultant force vector (F_R) that is directed dorsally and anteriorly, a component of which is thrust (thrust is directed in the horizontal plane, in the direction of animal movement). Movements of the tail result in a reactive force (F_{REACT}) causing net water displacement that is equal and opposite in direction to the resultant force vector. The heavy lines in the dorsal and posterior view depict the dorsal edge and the trailing edge of the tail respectively. The direction of movement of the beating tail is indicated by the dashed arrows (dorsal and posterior views). Note, in the posterior view, the difference between the two models in the ventral lobe angle with respect to the horizontal.

of small shark species. Although Alexander (1965) did not simulate the oscillatory nature of the *in vivo* tail beat and his experiments lacked the potential for intrinsic muscular control of the angle of the tail by the swimming shark, he was able to conclude that the lift produced by the tail movements increased with increasing tail size (relative size of both the terminal and ventral lobes) and with increasing velocity.

In 1976, a new model of heterocercal tail function in sharks was presented by Thomson on the basis of his observation that the ventral lobe did not appear to lag behind the terminal lobe, as expected in the classical model (Thomson, 1976; also see Thomson and Simanek, 1977; Thomson, 1990). Thomson (1976) obtained films of sharks swimming in an aquarium and described the ventral lobe as leading the terminal lobe throughout much of the tail-beat cycle. Thomson (1976) developed a model which predicted that the resultant force acting on the tail should be directed anteriorly and slightly ventrally through the shark's center of gravity (Fig. 1). Resolving the lift and drag vectors on the basis of this prediction shows that the lift force should be directed ventrally and be small in magnitude, while the drag force is directed anteriorly (Fig. 1). The water pushed by the tail should be directed in an equal and opposite direction to the resultant force vector, i.e. posteriorly and dorsally.

Although there have been some difficulties with Thomson's interpretations of tail function, his original *in vivo* kinematic observations of tail movement are contrary to the classical interpretation of heterocercal tail function, but have remained unexamined and are now entering the textbook literature (McFarland *et al.* 1979; McGowan, 1991; Videler, 1993). Blake (1983) discussed Thomson's model and concluded that if the force resulting from the tail beat were oriented through the center of gravity of the shark, the shark would not be in rotational equilibrium (owing to the now unopposed torque generated anteriorly at the pectoral fins). Additionally, while the resultant force shown in Fig. 1 corresponds to that presented by Thomson (1976), our depiction of the lift and drag vectors differs slightly from his analysis. Thomson's original model indicated that the lift vector produced by the tail should be dorsally and anteriorly directed at an angle that compensated for the angle of inclination (the amount by which the tail is tipped dorsally) of the tail as it beats. However, lift vectors are typically depicted as being perpendicular to the path of motion and do not change direction as a hydrofoil rotates along its axis: according to Thomson's model, the tail lift vector changes direction as the tail changes orientation even though the path of motion remains the same. Hence, in Fig. 1, we present an orientation of lift and drag vectors consistent with the central point of Thomson's model: that the resultant force is directed through the shark's center of gravity. With such corrections, a viable model remains that may explain the function of the heterocercal tail, and this model has yet to be tested.

In this paper, we provide a detailed kinematic analysis of heterocercal tail function in one species of shark, the leopard shark *Triakis semifasciata*. We present a three-dimensional analysis of tail kinematics that allows us to distinguish between the predicted kinematic patterns of the two models, and we

determine which model (classical or Thomson's) best explains the function of the heterocercal tail.

Materials and methods

Experimental subjects and protocol

Specimens of the leopard shark *Triakis semifasciata* Girard were obtained from the shallow surf zone off the coast of southern California. They were maintained on a diet of frozen squid and smelt, and held for a minimum of 1 month before beginning experiments. All individuals were housed together in a 400 l tank maintained at a temperature of 18±2 °C.

Four individuals with an average total length (L) of 35.0 cm (range 30.7–38.7 cm) were video-taped swimming at $1.2\,L\,s^{-1}$ in a calibrated flow tank (Fig. 2) maintained at the same mean temperature as the holding tanks (18±0.5 °C). This same apparatus was used previously by Jayne and Lauder (1994, 1995), who provide further details of this equipment. The working section of the flow tank that housed the swimming sharks measured 28 cm×28 cm×82 cm. Care was taken to keep each shark swimming in the center of the flow tank (not less than 4 cm from the walls or tank bottom) so that wall effects could be minimized. We calculated gap:span ratios according to the procedures outlined by Webb (1993), which provide a quantitative measure of possible wall effects (wall effects disappear as the gap:span ratio approaches 3). For the experiments reported in this paper, the gap:span ratio for all individuals was 2.4 or greater, indicating that wall effects are likely to be negligible. Data were only collected when the speed of the sharks matched the flow velocity.

Data were collected by video-taping the tail at 250 fields s^{-1} using a NAC HSV-500 high-speed video system. Two video cameras were used simultaneously to record two views, lateral and posterior, in order to calculate the movement of selected points on the tail in three dimensions (Fig. 2). The posterior view was obtained by aiming a camera at a front-surface mirror angled at 45 ° and placed in the flow at a distance of between 0.6 and 1.0 L behind the swimming shark (mean distance behind the trailing tail edge was 0.78 L; range 0.60–1.02 L). The lateral and posterior images were scaled equivalently using marked grids and a reference scale placed in the flow at the location of the tail (prior to beginning experiments). Output from the two cameras was combined on a split screen (Fig. 2). In addition, during separate experiments, a front-surface mirror placed at 45 ° beneath the flow tank allowed for a direct ventral view of the swimming shark. The tank was backlit by two 500 W photoflood lights, and additional side lighting on the tail was provided by four high-intensity fiber-optic lights.

A preliminary analysis was conducted to determine whether there was any effect of the posterior-view mirror on tail kinematics. The four sharks were video-taped swimming from a ventral view to allow for measurement of tail-beat frequency and amplitude both with and without the posterior-view mirror in place. Sharks were video-taped either with or without the mirror using the same criteria as above (for steady swimming and positioning) until four independent, replicate beats were

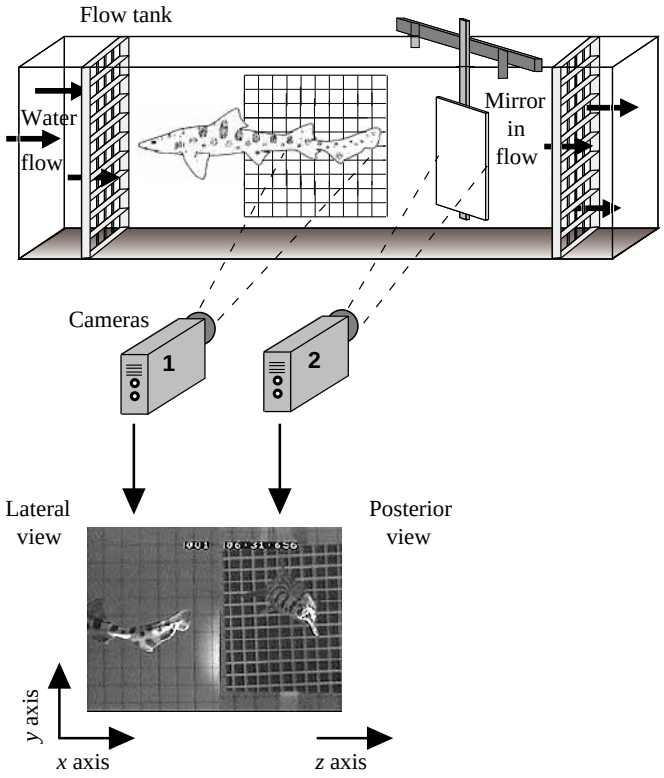

Fig. 2. Schematic diagram of the working section of the laboratory flow tank in which sharks were video-taped using two video cameras. Camera 1 provided a lateral view of the swimming animal and allowed for analysis in the x and y dimensions. Camera 2 provided a simultaneous posterior view (*via* a mirror in the flow) and allowed for a three-dimensional analysis by making movement in the z dimension visible. The image of the shark is enlarged for clarity. Sample images are also shown.

obtained from each individual. The order of introduction or removal of the mirror was alternated such that two individuals started their swimming with the mirror in position and two started without the mirror to ensure that length of time in the tank did not confound any possible mirror effect. We used a two-factor multiple analysis of variance (MANOVA) to test the random effect of individual and the fixed effect of mirror (with or without). The statistical results indicated that the mirror had no detectable effect on the mean amplitude or frequency of shark tail beats for any individual, with power greater than 80 % at all levels (Zar, 1984). Dye-stream injections of Methylene Blue video-taped at 250 fields s^{-1} also indicated that the mirror's interference with water flow had dissipated within one mirror width upstream. Therefore, we conclude that the presence of the mirror in the flow tank had little effect on tail kinematics.

Kinematics

Video footage of four replicate beats was scaled (in cm) according to reference grids, and images were digitized using a custom-designed digitizing program. With this program, the space in which the shark is swimming is divided according to

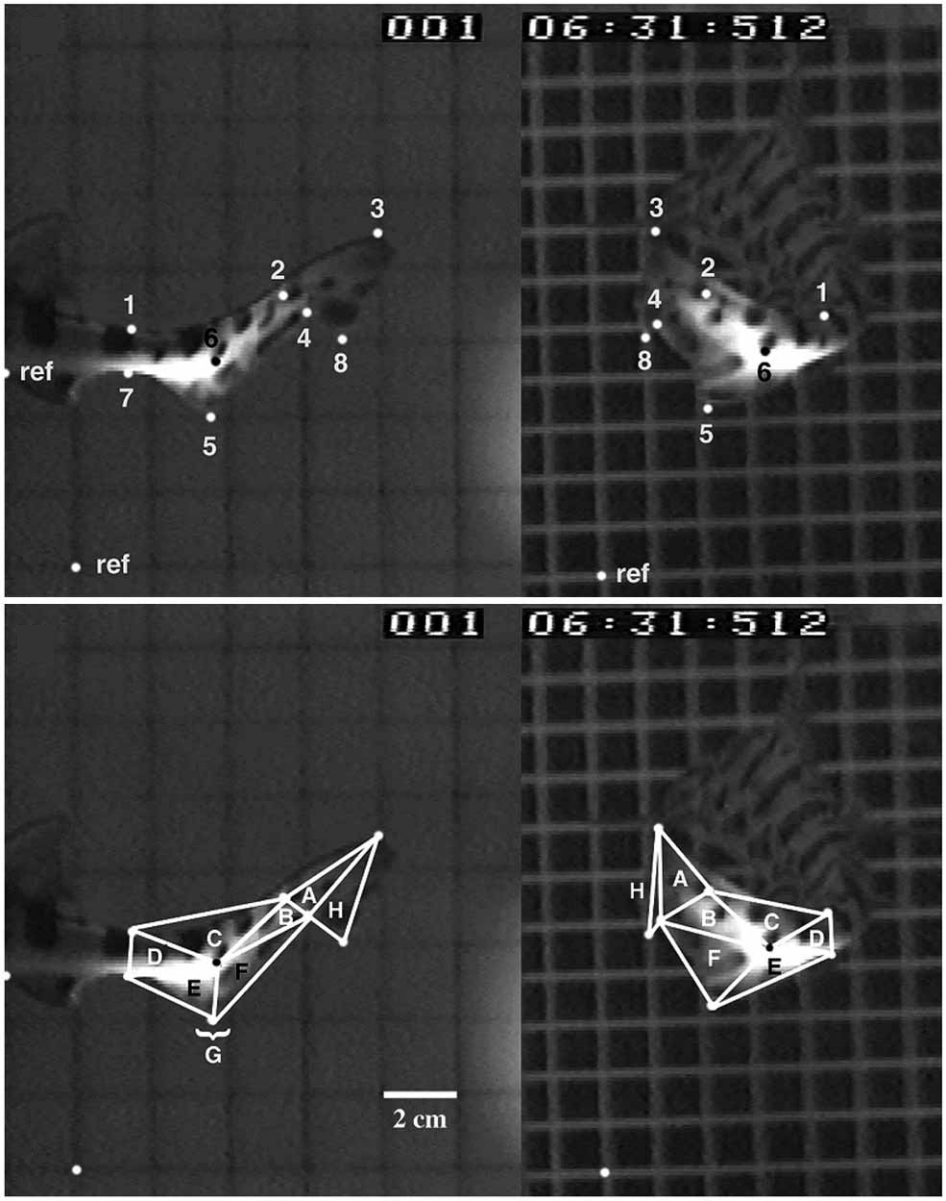

Fig. 3. Images from the two-camera video recording system with the landmarks (1–8) shown in both the lateral and posterior views (above), and the points joined to form the triangles (A–H) for analysis, shown below. Points marked 'ref' were digitized as reference points on the body and background. Both views were identically scaled using the grid in the lateral view (1 box = 2 cm), the smaller grid visible in posterior view is the smaller upstream baffle reflected in the mirror, towards which the shark is swimming.

a standard Cartesian coordinate system, and the position of any particular point in time can be given a value according to that system. The origin of the coordinate system was the lower left corner for the *x* and *y* dimensions and the lower left corner of the posterior image for the *y* and *z* dimensions (Fig. 2). The *y* dimension from the posterior view was redundant and the coordinate data were deleted from the analysis, leaving *x*, *y* and *z* coordinate data for any point.

Eight points on the shark tail (points 1–8; Fig. 3) were digitized and followed through replicate beats. These points were recognized by permanent landmarks on the sharks, and care was taken to keep them as consistent as possible among sharks. Points digitized were at the base of the second dorsal fin (point 1), a spot just anterior to the terminal lobe (point 2), the dorsal tip of the terminal lobe (or the tip of the tail; point 3), the ventral notch (below the terminal lobe; point 4), the ventral tip of the ventral lobe (point 5), a spot near the center of the tail where the vertebral column bends dorsally into the tail (point 6), the margin of the caudal peduncle directly ventral to point 1 (point 7), and the ventral tip of the terminal lobe (point 8). A single beat was defined as the complete lateral (*z*) excursion (from one extreme to the other and back again) of point 3.

Video fields collected at 250 fields s^{-1} were down-sampled such that every sixth frame was digitized: thus, analyzed frames were 0.24 ms apart. The data were smoothed using a binomial smoothing function (Macintosh IGOR Pro, Wavemetrics Inc.) to reduce the effect of small digitizing errors on subsequent calculations. The excursions, or the length of the path of travel during a beat, of each of the points in all dimensions (*x*, *y* and *z*) were determined. The timing of the excursion of each point in the *z* dimension (with the exception of point 7 whose *z* excursion, by convention, was the same value as the excursion of point 1) was analyzed by calculating

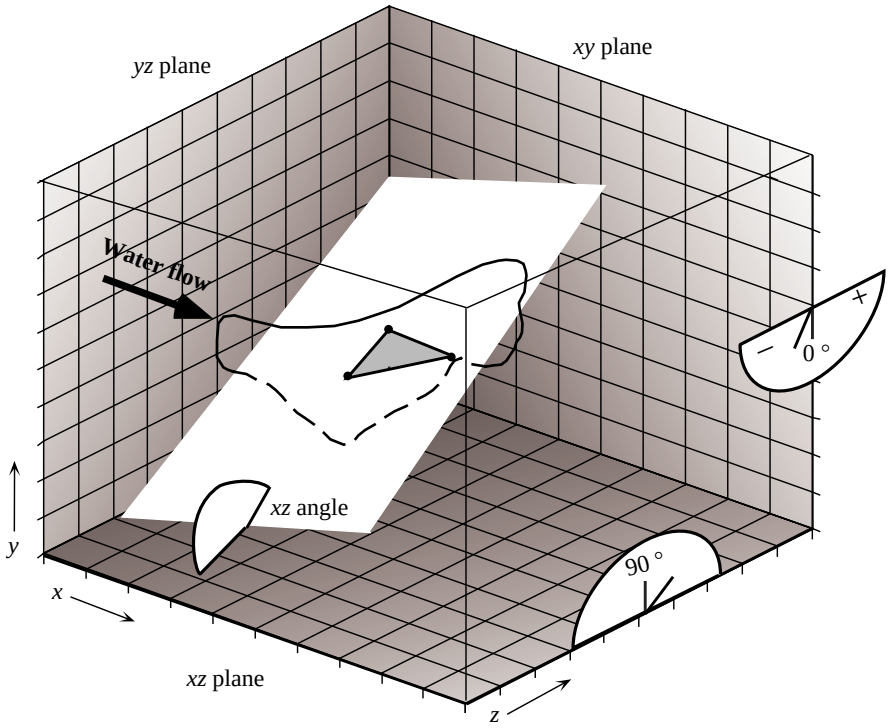

Fig. 4. Schematic representation of the shark tail in three-dimensional space at a static point in time. The reference planes are labeled. The floor of the 'box' is the *xz* plane. A representative triangle on the shark's tail in a theoretical position relative to the 'box' (not conforming to any particular model) is shown. The plane of this triangle has been extended to intersect with each of the three reference planes. The angle this plane makes with the *xy* and *xz* planes has been indicated on the edge of those planes. The *xy* angle would be considered negative by our convention, 0 ° being parallel to the plane. The *xz* angle shown would be obtuse, or greater than 90 °, as would the *yz* angle (the tail is leaning towards the shark's right), 90 ° being perpendicular to this plane. Visualization of the *yz* angle has been eliminated for clarity.

phase lags, or the timing of maximal lateral excursion for each point relative to the timing of maximal lateral excursion for point 3. Phase lags were expressed in terms of per cent cycle time. A negative value for phase lag means that a point is reaching its maximum lateral excursion before point 3 reaches its maximum on the same side. The eight points were joined to create triangular surfaces (Fig. 3; triangles A–H) whose three-dimensional movements could be calculated as described below.

For each time digitized, the angle of orientation of each triangle was determined by calculating the angle it made with each of three reference planes: sagittal (*xy*), transverse (*yz*) and frontal (*xz*). These planes can be thought of as the walls of a box or tank that define a three-dimensional space for movement of the tail (Fig. 4). Thus, the sagittal plane is equivalent to the side of the flow tank parallel to the swimming shark (visible as the lateral or *xy* view through camera 1; see Fig. 2). The transverse plane is represented by the front wall of the tank towards which the shark is swimming and which is visible as the posterior or *yz* view through camera two; see Fig. 2). The frontal plane (*xz*) is equivalent to the floor or bottom of the tank. Each triangular element of the tail defines a plane that can be extended until it intersects with each of the three reference planes, and it is these planar angles of intersection that were calculated for each triangle (Fig. 4).

Intersection with both the *xz* and the *yz* planes is defined in terms of angles greater or less than 90 °, with an angle of 90 ° being perpendicular to the plane (Fig. 4). By our convention, an obtuse angle would be created between the tail and the *xz* reference plane, for example, if the dorsal (upper) apex of the triangle were oriented farther to the right (a larger *z* coordinate value) than the lower apices, as shown in Fig. 4. In terms of the entire tail, this condition would be met if the terminal lobe were leading the ventral lobe of the tail during a beat to the right. The angle of intersection with the *xy* plane is defined as being greater or less than 0 °, with an angle of 0 ° being parallel with that plane. As in the above example, an angle between 0 and –90 ° would be created if a triangle were tipped such that the dorsal portion of the tail intersected the *xy* plane before the ventral portion of the tail (Fig. 4).

Movement of tail points and surfaces is difficult to visualize in three dimensions. In order to illustrate tail surface motion better, we represent the movement of each triangular component of the tail at a given instant in time as a three-dimensional scaled movement vector (see Fig. 10). In order to calculate the movement vector magnitude, we used the three-dimensional area of each triangle (*A*, taken as the maximum triangle area calculated during a full beat, because apparent area in any one plane will underestimate true area since tail triangles are not typically oriented parallel to any one plane) multiplied by water density (ρ) and the square of the velocity of the centroid of that triangle (u^2). This generated a vector in three-dimensional space with a magnitude (*F*) in units of newtons ($F=\rho A u^2$; see Vogel, 1981). The base of each vector was placed at the centroid of each triangle, and vectors were oriented normal to the surface of that triangle. The velocity used in the calculation of vector length was the component of centroid velocity along the normal to the triangle surface. At each point in time, movement vectors for each triangle were summed to calculate the total scaled vector magnitude resulting from tail motion. This vector is plotted as originating from the centroid of triangle B.

Vector magnitude oscillates over time as the tail moves through different stages of a beat, either between zero and a

large (positive or negative) number, or from positive to negative in the case of the *z* dimension. Mean magnitude in each dimension was calculated as the average of vector magnitudes over an entire beat, and this provided an indication of the average direction of triangle movement during that beat. Vector phase lags were calculated by comparing the time of the maximum value of the movement vector with the timing of maximum lateral excursion of point 3, expressed in terms of per cent cycle time. A negative value for vector phase lag means that maximal movement vectors are generated before point 3 reaches its maximum excursion to the side.

Statistical analyses

Parametric statistical analyses were performed using the Macintosh computer programs SuperANOVA and Statview on untransformed data.

The excursion of each landmark (in cm) on the tail in each of the three dimensions was compared among individuals using a mixed model, two-factor MANOVA with individual and point (1–8) as effects, and excursion in each dimension (*x*, *y* or *z*) as multiple dependent variables. Within each dimension, significant differences within the fixed effect (point) were tested using multiple *post-hoc* ANOVAs, with significance levels corrected for performing multiple tests. (The proper alpha value for determining significance was calculated using the conservative method of dividing the standard alpha level of 0.05 by the number of tests performed, see Zar, 1984.) Significance levels were always either highly significant or clearly not significant, so the conservative nature of our correction did not affect our conclusions. Bonferroni/Dunn *post-hoc* tests for each ANOVA were used to perform pairwise comparisons to identify specific point effects (all individuals) or to determine which points were significantly different from one another in their excursions. This *post-hoc* test automatically adjusts significance levels for the number of comparisons performed.

The phase lags of each point (expressed in per cent cycle time) were compared among individuals using a mixed-model, two-factor ANOVA with point and individual as main effects. A Bonferroni/Dunn *post-hoc* test on the fixed effect of point was used to perform pairwise comparisons (all individuals) to determine which phase lags were significantly different from one another. To determine whether the phase lags were significantly different from zero (a phase lag of zero indicates no lag relative to point 3), one-sample *t*-tests were performed comparing the phase lags of each point (all individuals) with a hypothesized mean of zero. Significance levels for this analysis were adjusted as above for performing multiple *t*-tests.

Similarly, the mean scaled vector magnitude (in N) in each dimension was compared with a hypothesized mean of zero in multiple one-sample *t*-tests. The vector phase lags, relative to point 3 (expressed in per cent cycle time), were compared among individuals and dimensions (*x*, *y* and *z*) using mixed-model, two-factor ANOVAs. A Bonferroni/Dunn *post-hoc* test on the fixed effect of dimension was used to perform pairwise comparisons (all individuals) to determine which phase lags were significantly different from each other. To determine whether the vector phase lags were significantly different from zero, one-sample *t*-tests were performed comparing each dimension's vector phase lag (all individuals) with a hypothesized mean of zero. Again, for this analysis, significance levels were adjusted for performing multiple *t*-tests.

Dye-stream injections

Dye-stream injections were used to visualize the direction of water deflection by the moving tail. Dye was injected using a fine-gauge hypodermic needle bent at 90° near the tip to allow dye to be injected in the same direction as water flow so that artificially introduced turbulence within the dye stream was reduced. The stream of dye was injected alongside the swimming shark just posterior to the pectoral fins, to prevent interference from the fins and lateral to the body. Dye injections were timed so that a steady longitudinal stream of dye was generated. As the tail beat across the dye stream, dye was deflected in the direction of water movement.

Results

Kinematics

As the tail beats from left (Fig. 5A) to right (Fig. 5F), points 3 and 8, defining the trailing edge of the terminal lobe, appear to move in phase throughout the beat; thus, the trailing edge of this lobe remains nearly vertical. In posterior view, the ventral lobe often appears to lead lateral (*z* dimension) movement of the terminal lobe (Fig. 5C,D). As the tail continues its beat to the right from this position, the trailing edge of the tail reaches nearly a vertical position in which the terminal and ventral tail tips are aligned (Fig. 5E). Finally, in Fig. 5F, the tail has begun to beat back to the left.

Table 1 provides values for the excursions (movement from one extreme to the other) of the points on the tail for all individuals in each dimension (*x*, *y* and *z*). The MANOVA testing for individual and point excursion differences in each dimension revealed highly significant differences in excursion among points (d.f.=21, 55; Wilks' lambda = 11.778; P=0.0001). Bonferroni/Dunn *post-hoc* pairwise comparisons indicated that significant differences among excursions of points were most common between points greater distances from one another on the tail (Table 1), with more-posterior points having significantly greater excursions. For example, two points on the posterior margin of the tail, 3 and 8 (see Fig. 3), do not have significantly different excursions in the *z* dimension (as seen in Fig. 5, posterior view), while point 3 travels a greater distance than point 5 in its path of oscillation from side to side. Although this MANOVA detected significant individual effects (d.f.=9, 228; Wilks' lambda = 4.968; P=0.0001), the interaction term was not significant.

A plot of the *z* excursion of the most posterior points on the tail illustrates the phase lag among points in this dimension (Fig. 6A). ANOVA indicated that phase lags for each point

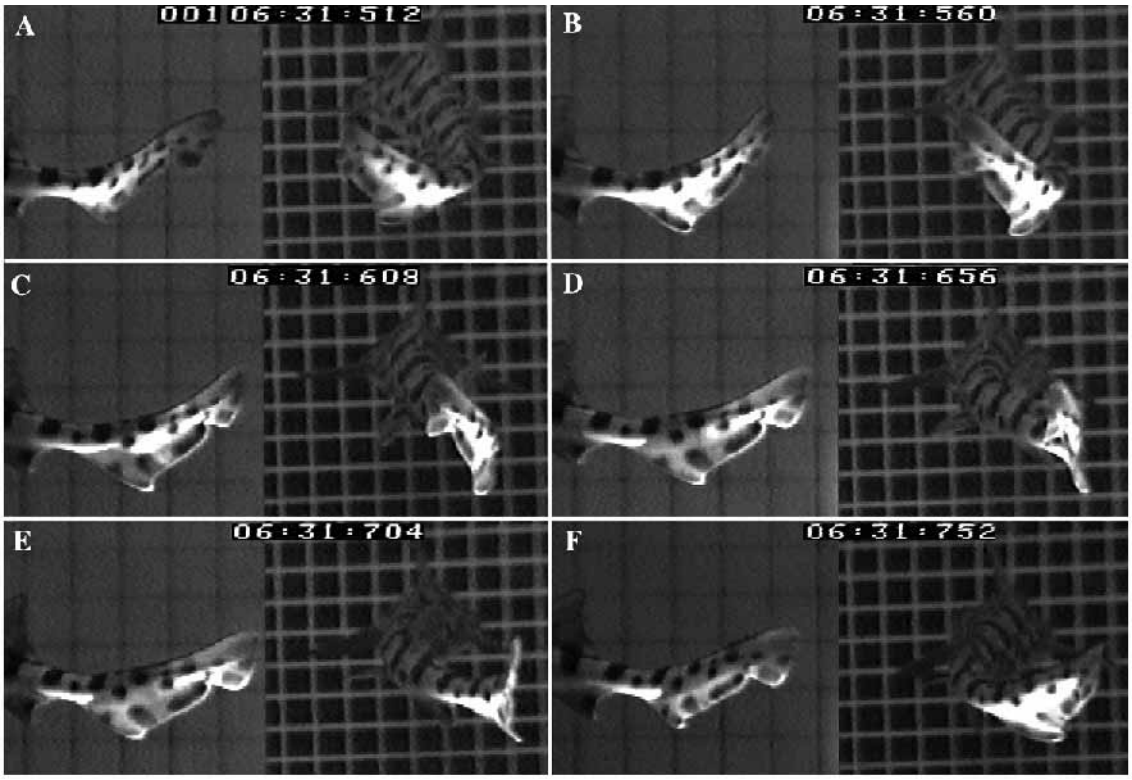

Fig. 5. Composite video sequence of the tail beating from the leftmost extreme (A), crossing the midline of the beat (C and D), and beating to the rightmost extreme or maximum lateral excursion (reached in E and F). In F, the tail has started its beat back to the left. Images have been cropped and contrast-enhanced for clarity using Adobe Photoshop. Times for each image are shown at the top, with the last three digits indicating elapsed time (in ms).

Table 1. *Mean length of excursions for points 1–8 (see Fig. 3) on the tail pooled for all individuals*

	Excursion distance (cm)					
Point	*x* dimension	Significant difference*	*y* dimension	Significant difference*	*z* dimension	Significant difference*
1	0.70±0.22	3, 5	0.55±0.25	5**, 4**, 8, 3	4.11±0.49	6***, 2, 4, 8, 5, 3
2	0.86±0.26	5	0.64±0.24	8**, 3	5.93±0.64	5**, 1, 3
3	1.10±0.26	1, 7	0.83±0.33	4**, 7, 1, 6, 2	7.22±0.72	1, 6, 2
4	0.93±0.26	5	0.70±0.25	6***, 7**, 1**, 3	6.30±0.63	1, 6
5	1.33±0.27	1, 2, 4, 6, 7, 8	0.68±0.28	7**, 1**, 3	6.95±0.52	2**, 1, 6
6	0.86±0.20	5	0.58±0.24	4***, 8, 3	5.08±0.55	1***, 4, 8, 5, 3
7	0.74±0.23	3, 5	0.55±0.23	5**, 4**, 8, 3	4.11±0.49	NA
8	0.89±0.26	5	0.76±0.31	2**, 7, 1, 6	6.32±0.70	1, 6

Values are means ± S.D. and dimensions are given in cm.

Significant differences among excursions of points were tested using a Bonferroni/Dunn *post-hoc* (pairwise) comparison.

Points that are significantly different from each point in column one are listed for each of the three dimensions in order of decreasing *P* value. For example, point 1 has a mean excursion among individuals of 0.70 cm in the *x* dimension, which is significantly smaller than those of points 3 and 5 which have mean excursions of 1.10 and 1.33 cm, respectively, in the *x* dimension.

*P<0.0001 except when otherwise noted; **P<0.001; ***P=0.0017.

NA, not applicable.

measured in the *z* dimension were significantly different (Fig. 6B; d.f.=5, 15; F=453.351; P=0.0001), as were individuals (Fig. 6B; d.f.=3, 72; F=10.255; P=0.0001), but without significant interaction. Bonferroni/Dunn *post-hoc* tests indicated that the phase lags of all points were significantly different from one another (P<0.0001), except for points 5 and 2; hence, points 5 and 2 moved in phase. One-sample *t*-tests showed that, for all individuals combined, phase lags were

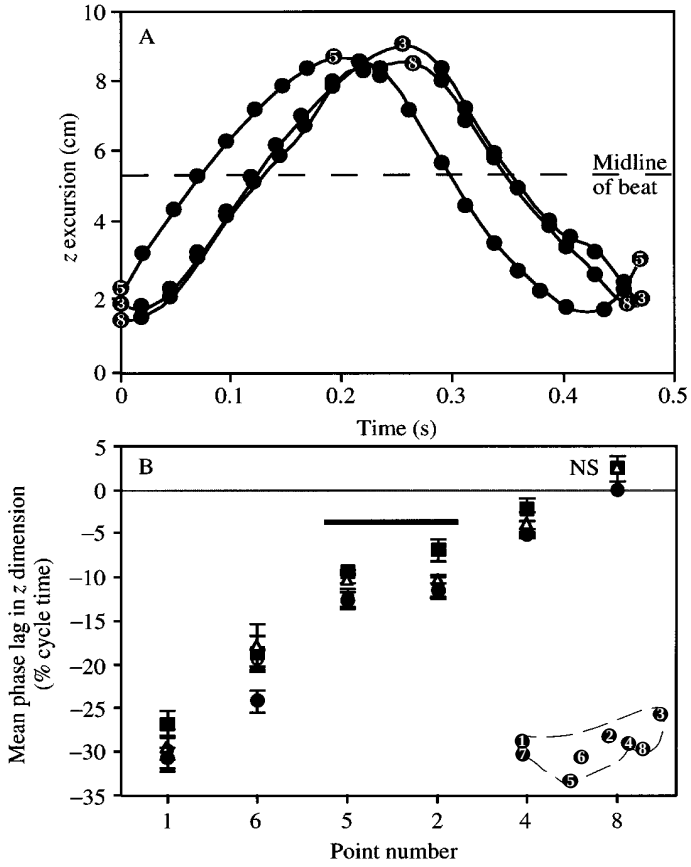

Fig. 6. (A) Excursion of points at the posterior margin of the tail (points 3, 5 and 8; see Fig. 3 and inset in B) through time showing the phase lags among points (data are from one representative individual). The path of the points from a minimum *z* value to a maximum *z* value and back represents a complete sweep of the tail from one extreme to the other and back again. Data points are shown 48 ms apart for clarity. (B) The mean phase lag (± S.E.M.) of each of the points on the tail relative to point 3 (in percentage cycle time) in the *z* dimension for all four individuals. A negative phase lag indicates that a point reaches its maximal excursion before point 3. For all individuals combined, points that are not significantly different from zero (all $P>0.0001$, one-sample *t*-tests with Bonferroni correction), or have no phase lag, are indicated by NS. Points not significantly different from one another (2 and 5) are indicated by a bar. The positions of the points on the tail are indicated in the inset.

significantly different from zero (d.f.=15; all $P<0.0001$) except for point 8 ($P=0.0412$), indicating that all points except 8 reached their maximal excursions before point 3, and that point 8 was not out of phase with point 3.

The planar angles created by the surfaces of the triangles with respect to the three reference planes are shown in Fig. 7. Note that, although we show the lateral excursion of point 3 for reference (an indicator of a complete tail beat), point 3 is not contained in *all* triangles and thus its excursion is not an accurate indicator of the position of some triangles in the beat over time. At the start of a tail beat to the right, all triangles are oriented at an angle greater than or equal to 90 ° with the *xz* plane (the bottom of the flow tank). Initial movement at an angle greater than 90 ° indicates that the most ventral vertex of each triangle was trailing as the triangle moved laterally. As the tail continues to beat to the right, large portions of the tail (triangles A, B and H) maintain an angle of greater than 90 ° angle to the *xz* plane. Triangle C, however, rapidly achieves an angle of less than 90 ° to the *xz* plane, followed by triangle G, representative of the ventral lobe of the tail. These positions are maintained as the tail passes the midline of the beat (approximately 0.13 s). As the tail approaches the end of its excursion to the right (as indicated by the path of point 3), all angles begin to approach 90 °, indicating a more perpendicular orientation with the *xz* plane. Most triangles, however, do not change their orientation (from >90 ° to <90 °) until the tail reaches its lateral extreme and begins to move back in the opposite direction (approximately 0.25 s). Triangle D, the small element at the anterior end of the caudal peduncle, maintains a 90 ° angle throughout the beat.

The *yz* angle (Fig. 7) is an accurate reflection of the lateral (*z* dimension) movement of any given triangular surface. As any individual triangle moves from left to right, the *yz* angle will increase from an initial minimum value of less than 90 ° (given our measurement conventions; see Fig. 4). Triangles pass through 90 ° at the middle of the beat as they become perpendicular to the *yz* plane and finally reach a maximum value of greater than 90 ° as they conclude their movement to the right. All triangles were initially oriented at angles of less than 90 ° to the *yz* plane, as the more posterior vertex of each triangle trails behind the most anterior vertex during the tail beat (as indicated by the larger excursions of the more posterior points and the significant phase lags among points). Triangles varied, however, in the time at which they achieved perpendicular orientation to the *yz* plane (Fig. 7).

Movement vectors associated with each triangle oscillated in magnitude throughout the tail-beat cycle. In Fig. 8, we depict the magnitudes of the movement of each of the tail triangles in all three dimensions. For all triangles in the *x* dimension, scaled vector magnitude builds to a large, positive value early in the tail-beat cycle (just after the maximum lateral excursion from the previous beat) and then slowly declines to zero as the tail beats towards the opposite side. Only very rarely did triangle orientation and velocity produce a small, negative component, indicating that the *x* movement vector pointed into the flow (not seen in the beat plotted in Fig. 8). For example, triangle A (which contains point 3 as one of its vertices) shows maximum posterior movement 0.05 s into the beat, just after the maximum lateral excursion of point 3 at approximately 0.04 s. As the tail beats back towards the opposite side, posteriorly directed movement is reduced, as might be expected on the basis of the triangle orientation (angle with the *yz* plane) discussed above, and does not build again until the opposite maximum lateral excursion is reached.

Peak *y* and *z* magnitudes also occur early in the tail-beat cycle and approach zero as the tail crosses the midline of the beat (Fig. 8). Peak *y* magnitude was usually negative, indicating that the *y* vector was pointed ventrally relative to the centroid of the triangle, as indicated by the angles that most of

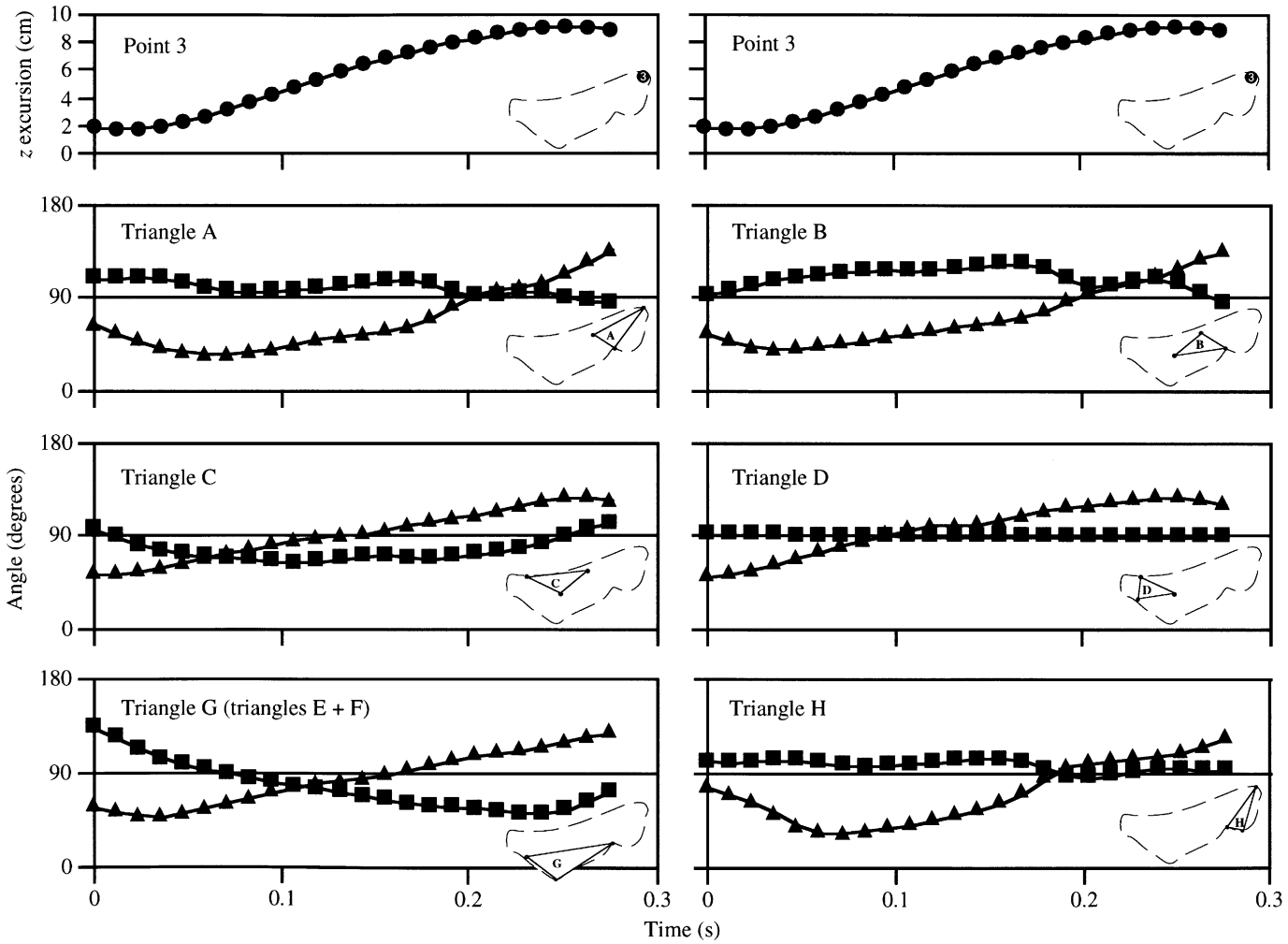

Fig. 7. Angles created between triangular segments of the tail and two reference planes (■ *xz*, ▲ *yz*) for one individual during a half tail-beat to the right. The *xy* angle is not shown for clarity and may be calculated from the values of the other two angles if desired. The excursion of point 3 has been added (top) for reference. All individuals conformed to the patterns shown.

the triangles made with the *xz* plane. The notable exceptions to this were triangles C and G, which tended to have periods of small dorsally directed (positive) *y* vectors (and were oriented at ⩽90 ° to the *xz* plane at the corresponding times). Maximal vector magnitudes (reflecting greater triangle area and velocity) occurred in triangle G, which typically showed large negative *y*-vector magnitudes early in the beat. The period of positive vector magnitude was not always present. *z*-vector magnitude oscillated around zero, as would be expected given that the tail was beating back and forth (Fig. 8).

Fig. 9 shows the pattern observed when the movement vectors produced by each triangle are summed over the entire tail and re-scaled to a percentage of the maximum magnitude produced during that beat. Table 2 gives the specific values. Like the individual triangles shown in Fig. 8, the overall movement in the *x* dimension produced by the tail peaks just after the maximum lateral excursion of the tail centroid. There was a significant positive phase lag of this peak for all individuals relative to the excursion of point 3, meaning that the generation of maximal *x*-vector magnitude occurred significantly later than the maximum lateral excursion of point 3 (one-sample *t*-tests of the null hypothesis: phase lags = 0; all $P<0.0001$, Table 2). Like the individual triangles, as the tail crosses the midline of the beat, the magnitude of the movement vectors in the *x* dimension decreased. Summation of this pattern across all triangles which reach their minimum magnitudes at slightly different times (see Fig. 8) resulted in a minimum value that does not reach zero. The mean scaled vector magnitude over time in the *x* dimension was significantly positive (one-sample *t*-tests of the null hypothesis: mean scaled vector magnitude = 0; all $P<0.0001$, Table 2), indicating a significant posteriorly directed contribution to locomotion.

In summing the movement vectors for the individual triangles, a single unifying pattern was evident which describes the movement of the heterocercal tail in the *y* dimension. A large, negative peak was reached at approximately the same time as the maximum lateral excursion of the tail as indicated

Table 2. *Mean movement vector magnitude for all individuals in the* x, y *and* z *dimensions and phase lags of the peak vectors in each dimension relative to the tip of the tail*

Dimension	Mean vector magnitude (mN)	Peak movement vector phase lag (% cycle time)	Phase lag significant differences**
x	486.70±156.04*	7.21±2.31*	*y*
y	−144.06±68.95*	1.54±2.38	*x*, *z*
z	−2.712±96.06	6.80±2.30*	*y*

Values are means among individuals ± S.D.

Phase lags were subsequently compared with zero (to determine whether phase lag was significantly positive or occurred significantly later than the maximum lateral excursion of point 3) and with one another.

Statistical results were the same when individuals were analyzed separately.

*Significantly different from zero (P<0.0001, one-sample t-tests with Bonferroni correction).

**Significantly different from one another (all P=0.0001, Bonferroni/Dunn *post-hoc* on two-factor ANOVA).

by motion of point 3. No significant phase lag was detected for the time of peak *y*-vector magnitude (Table 2), indicating that peak magnitude occurred at same time as the maximum lateral excursion of point 3. This is corroborated by Bonferroni/Dunn *post-hoc* tests on the two-factor ANOVA which indicated that the peak negative *y* movement vector was generated significantly earlier than peak *x* movement (ANOVA; d.f.=3,9; F=298.401; P=0.0001, Bonferroni/Dunn *post-hoc* tests; P<0.0001, Table 2). The small positive contribution of triangle C to the *y* dimension were outweighed by the large negative contribution of triangle G, the ventral lobe, and the mean vector magnitude in the *y* dimension was significantly negative (for all individuals combined, Table 2), indicating a significant ventrally directed contribution to locomotion.

The peak *z*-vector magnitude (maximum or minimum) lagged significantly behind the maximum lateral excursion of point 3, and Bonferroni/Dunn *post-hoc* tests (on the above two-factor ANOVA) indicated that *z*-vector peaks occurred at the same time as the peak *x*-vector magnitude (Table 2). There was no individual effect on dimensional vector magnitude nor was there a significant interaction term. The oscillation of *z*-vector magnitude around zero generated a mean *z*-vector magnitude that was not significantly different from zero (Table 2), indicating that there is not significant lateral component to locomotion overall.

Fig. 10 shows a visual representation of the position of the tail and the pattern of triangle movement at the time of maximum overall negative *y*-vector magnitude (see Fig. 9). This figure is generated by placing the base of the resolved three-dimensional (i.e. the combined *x*, *y* and *z* contributions like those isolated in Fig. 8) scaled movement vectors for that time at the centroid of each triangle. The large vector produced by triangle G is apparent, reflecting the relatively high velocity and large surface area of this triangle at this time. The dorsal orientation (positive *y* magnitude) of the vectors produced by triangles C and D can also be seen in posterior view. This same image for the total three-dimensional scaled movement vector summed over the entire tail (i.e. the combined *x*, *y* and *z* contributions from Fig. 9, or alternatively, the sum of the vectors illustrated in Fig. 10) illustrates the large posteriorly and ventrally directed overall movement of the tail triangles at this time (Fig. 11).

Dye-stream injection

Dye stream injection showed that the tail deflected water flow ventrally (Fig. 12), at an angle of approximately 20°. A clear depression in the dye stream can be noted as a result of the tail's sweep through it. Dye injected lateral to the ventral lobe experienced a greater ventral angular deflection than dye injected lateral to the terminal lobe, which showed relatively little ventral angular deflection as a result of dorsal tail movement. This result was regular and repeatable; dye was never deflected dorsally by the tail.

Discussion

The tail-beat cycle

The classical and Thomson (1976) models of heterocercal tail function in sharks make specific and different predictions about the expected patterns of tail movement. The classical model predicts that the dorsal edge and terminal lobe of the tail should lead the ventral lobe as the tail beats. Thus, in a beat to the right, as our data are presented, the majority of tail triangles should be inclined at an obtuse angle (>90°) with the *xz* plane, so that water is directed ventrally and posteriorly. Thomson (1976) predicted specifically that the ventral lobe should lead the terminal lobe through a significant portion of the beat and that the tail should be inclined at an acute angle to the *xz* plane during a beat to the right (see Fig. 1, Thomson model). The classical model predicts that the *y* movement vectors from tail triangles should be significantly negative, while Thomson's

Fig. 8. Scaled movement vectors generated by each of the triangular segments of the tail for each of the three dimensions shown, relative to the *z* excursion of the tip of the terminal lobe (top) for the same individual during a half tail-beat. Although these were calculated in units of newtons, they have been expressed in terms of per cent of the maximum value. Thus, the height of each bar reflects the magnitude of the vector generated scaled to the maximum value generated during the beat for any triangle in that dimension. This maximum value was always generated by triangle G, the ventral lobe of the tail, composed of triangles E and F (note the different scale for triangle G), the only triangle whose movement reaches 100 %. Note that positive *x*-vector magnitudes reflect a vector pointing posteriorly, while a negative *x* value indicates that the vector points anteriorly (into the flow). Positive *z*-vector magnitudes indicate a vector pointing to the right, while negative *z*-vector magnitudes reflect a vector pointing to the left. Positive *y*-vector magnitudes reflect a vector pointing dorsally, while negative *y*-vector magnitudes indicate that the *y* vector points ventrally.

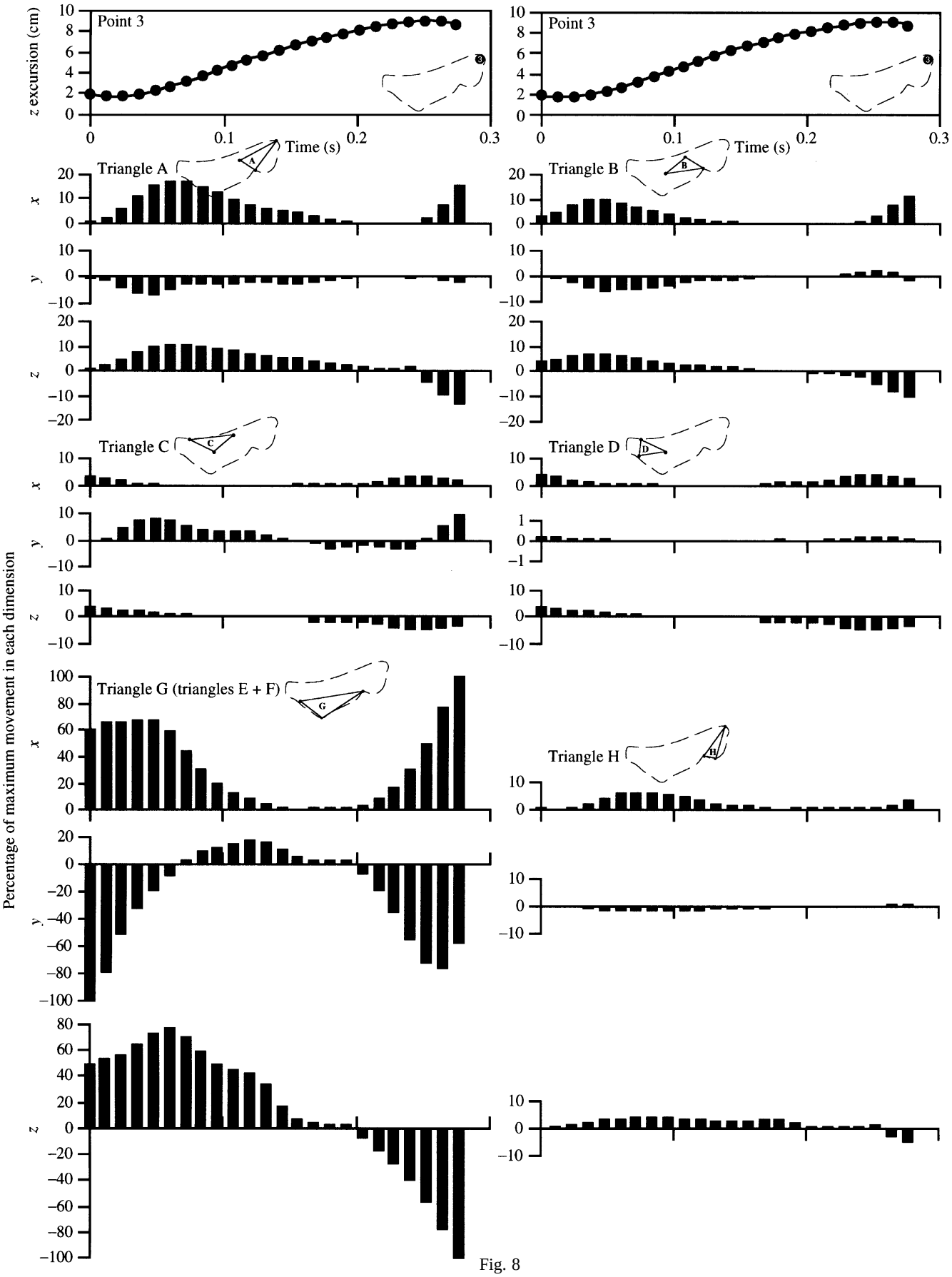
Point 3
z excursion (cm)
Time (s)
Triangle A
Triangle B
Triangle C
Triangle D
Triangle G (triangles E + F)
Triangle H
Percentage of maximum movement in each dimension
x
y
z

Fig. 8

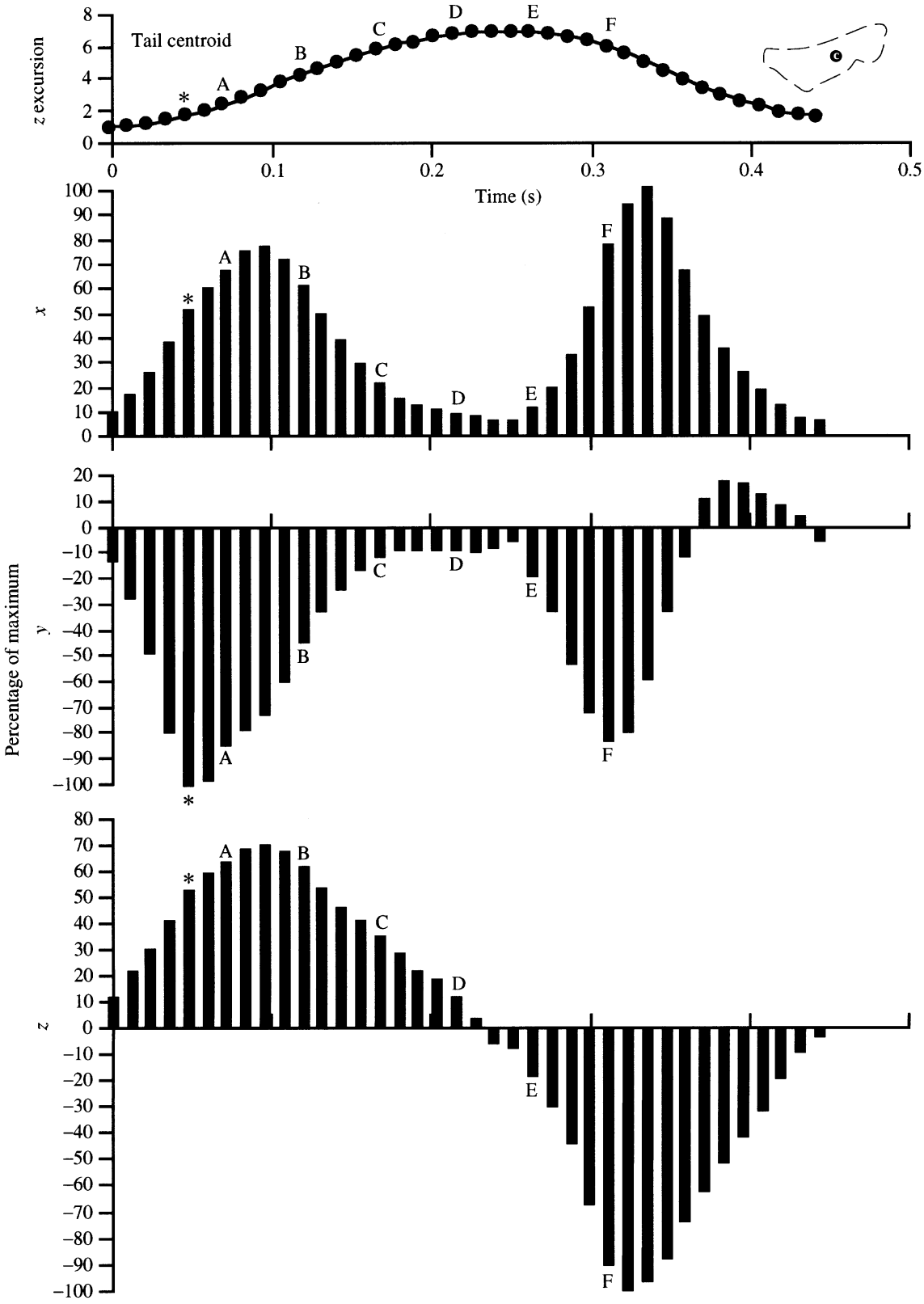

Fig. 9

model predicts overall positive values. Finally, the classical model predicts that water should be deflected posteriorly and ventrally by the tail, while Thomson's (1976) model predicts that water should be deflected posteriorly and dorsally.

Our data provide strong support for the classical model. Our three-dimensional analysis of tail kinematics indicates that many portions of the tail are, in fact, oriented at obtuse angles during a beat to the right. This is corroborated by the

Fig. 9. Scaled movement vectors summed over the entire tail (all triangles) in each of the three dimensions (below) shown relative to the *z* excursion of the center of the tail (approximated by the centroid of triangle B and marked c on the inset tail outline; above) for the same individual during a single tail beat. Letters A–F refer to the times of images A–F in Fig. 5. The asterisk refers to the time depicted in Figs 10 and 11, a time when tail position is similar to that shown in image F of Fig. 5. The times marked with an asterisk occur slightly before time zero depicted in Fig. 8. A slightly longer time period has been incorporated into this figure to allow for the visualization of an entire beat. Time has been re-scaled to zero at the start of the excursion of the tail centroid.

movement vectors, which show that tail triangles are moving in a manner likely to direct the water ventrally and posteriorly, not dorsally and posteriorly as Thomson's (1976) model predicted. As shown in Figs 9 and 11 and Table 2, the *y* component of triangle movement is significantly negative; when vectors are summed over all triangles, there are only brief periods when vector orientation is positive, the condition predicted by Thomson (1976). In addition, the dye-injection results demonstrate that the tail always deflects water posteriorly and ventrally. The angle of deflection (approximately 20 ° below the horizontal) closely matches the summed movement vector orientation for all tail triangles (Fig. 11), suggesting that the analysis of tail triangle surface orientation and path of motion provides a reasonable overall description of tail function.

Our kinematic data suggest that the majority of the vertical (*y*) component of water movement is generated by the tail early in the tail beat (as defined by lateral movement of the tip of the tail; point 3). As the tail tip reaches its maximal lateral excursion and begins to beat back to the right, all tail triangles are oriented at an angle of 90 ° or greater, suggesting that movement of the tail is directing water movement in a ventral and posterior direction. At this time, the entire tail is acting effectively as a single plate, inclined at an obtuse angle with the *xz* plane. As the tail tip sweeps towards the midline, first triangle C and later triangle G rotate into an acute angle with the *xz* plane, and differentiation of triangle orientation begins to occur. The magnitude of the scaled vector movement generated by the ventral lobe is actually much larger than that generated by the terminal lobe (see Fig. 10) as a result of the large surface area of the ventral lobe and its rapid velocity at this time. Although some triangles are oriented at an acute angle to the *xz* plane during portions of the tail beat, the area and velocity of these triangles are low and they do not contribute substantially to the dominant negative *y* movement vector magnitudes observed for the tail as a whole (see Fig. 11). For example, triangle G does show some periods of positive *y*-vector magnitude, indicating that the ventral lobe can be oriented at an acute angle to the *xz* plane as Thomson (1976) suggested. But this orientation does not occur during a time of high triangle velocity and it occurs when several other tail triangles are oriented at an obtuse angle to the *xz* plane. Overall, the dominant contribution to the negative *y* orientation

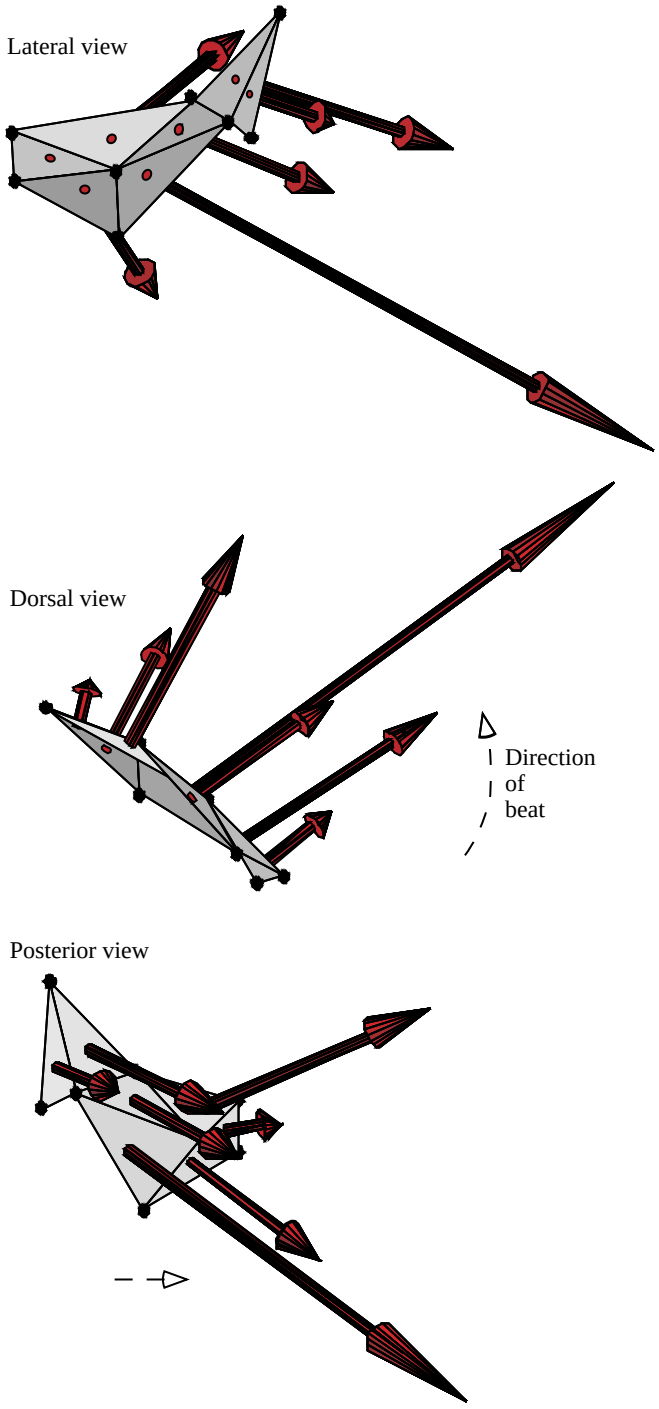

Fig. 10. Three-dimensional view of instantaneous triangle movement vectors for a single representative individual. Arrows represent the scaled vector magnitude for each individual triangle at the time of maximum overall negative *y* magnitude (see asterisk, Fig. 9), approximately 0.05 s into the beat as it is depicted in Fig. 9. The direction of the tail beat is indicated by the dashed arrows.

of the movement vectors is from the triangles representing the terminal and ventral lobes (triangles A, B, H and G). Triangles representing the central and anterior regions of the tail (C and D) show mostly positive *y*-vector magnitudes, but their relative

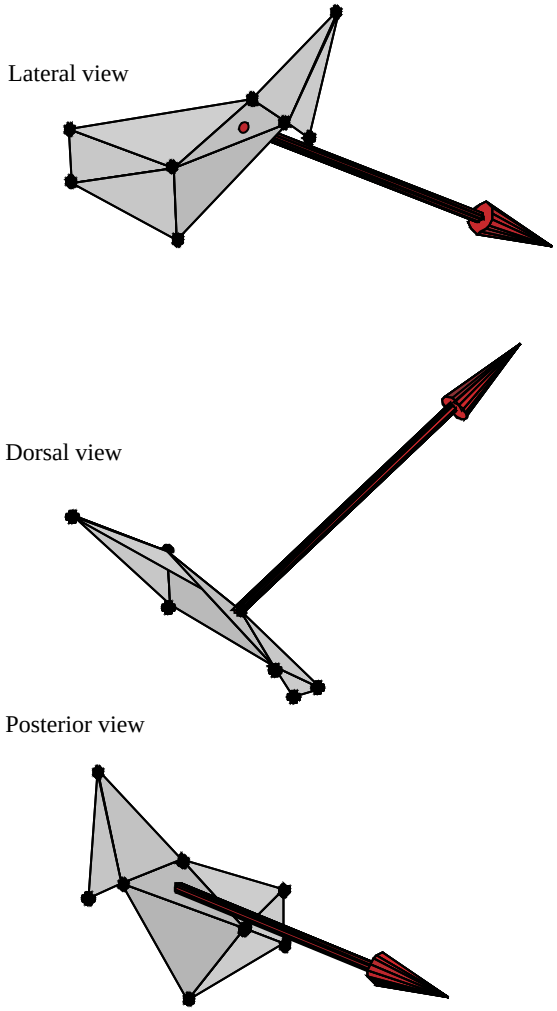

Fig. 11. Three-dimensional view of instantaneous triangle movement vectors (for one representative individual) summed over all triangles to produce the total scaled movement vector approximately 0.05 s into the beat depicted in Fig. 9, the time of maximum negative *y* magnitude (see asterisk, Fig. 9). Because all vectors shown in Fig. 10 have been summed to a single overall vector, this vector is no longer normal to any individual triangle. Note that this vector is directed significantly downwards (ventrally).

velocity is low and their total area is small; hence, kinematic data suggest that these tail regions contribute little to overall tail thrust.

We present the above data as 'movement vectors' as an aid to understanding the pattern of tail surface motion (kinematics). Although these vector magnitudes are expressed in units of newtons and give results that are mathematically very similar to the thrust calculations based on fish tail movement provided by Videler (1993), we do not consider these vectors to indicate either the pattern of fluid motion or reactive forces on the tail *per se*. Fluid flow around the fish tail, particularly a heterocercal tail with asymmetrical mass distribution around the horizontal axis, which moves in an unsteady oscillatory manner, is not likely to be accurately described by a steady-state analysis. Movement vectors, however, are quite useful tools for visualizing tail motion and, therefore, determining to what degree each model's movement predictions are supported.

Our data also show that the two lobes of the tail function differently in several respects. The terminal lobe (triangles A and H) remains nearly vertical (i.e. 90 ° to the *xz* plane) and travels through a significantly larger *z* excursion during the tail-beat cycle than the ventral lobe (triangle G). This results from the more posterior location of the terminal lobe, which must necessarily experience greater *z* excursions as a result of the traveling wave of body displacement moving posteriorly along the shark with increasing amplitude. The ventral lobe is considerably anterior to the terminal lobe and reaches its maximal lateral excursion significantly earlier in the tail-beat cycle (see Table 2). Overall, our data suggest that *z* excursions of points on the heterocercal tail of *Triakis semifasciata* (see Table 1) behave kinematically in accordance with expectations based on anterior–posterior position.

Re-evaluating the Thomson model

Why are our results so different from the predictions of Thomson, especially given that the posterior view of tail shape presented by Thomson (1976) appears to corroborate his model of tail function? The most significant difference between the studies is our extension of the study of heterocercal tail kinematics into three dimensions. Thomson used only the trailing edge of the tail as seen in posterior view to visualize tail function and to corroborate his proposed model of force generation. The major difficulty with this perspective is that it is the tail surface which generates thrust, and yet the surface of the tail is not visible when a posterior view is used alone. Our data show that using the posterior view of the trailing edge to estimate the three-dimensional orientation of the tail lobes may be very misleading. For example, the trailing edge reconstructed as points 3, 8, 4 and 5 (see Figs 3 and 5) gives the impression that the tip of the ventral lobe, point 5, leads the tail beat in the lateral (*z*) direction for most of the beat. Indeed, examination of the video image associated with the trailing edge shape in Fig. 5A seems to corroborate the view that the ventral lobe is inclined at an acute angle to the horizontal and might be acting to move water dorsally, as originally suggested by Thomson (1976). However, this inference would be incorrect for the early stages of the beat as the ventral lobe (triangle G) actually makes an obtuse angle with the horizontal at this time. The apparent acute angle of the ventral lobe in Fig. 5A results from reducing a three-dimensional tail to two dimensions. Point 5 is actually substantially anterior to points 3, 8 and 4 (and thus has a smaller *x*-coordinate value), as can be seen from a simultaneous lateral view (Figs 3 and 5). The edge of the ventral lobe thus *looks* as if it is inclined at an acute angle when in fact the three-dimensional coordinates for the triangle G vertices show that the surface of the triangle must be obtuse to the horizontal at this time. Hence, when this triangle moves laterally, the surface of triangle G would tend to impart a negative *y* (ventral) component to water near the tail. Only later

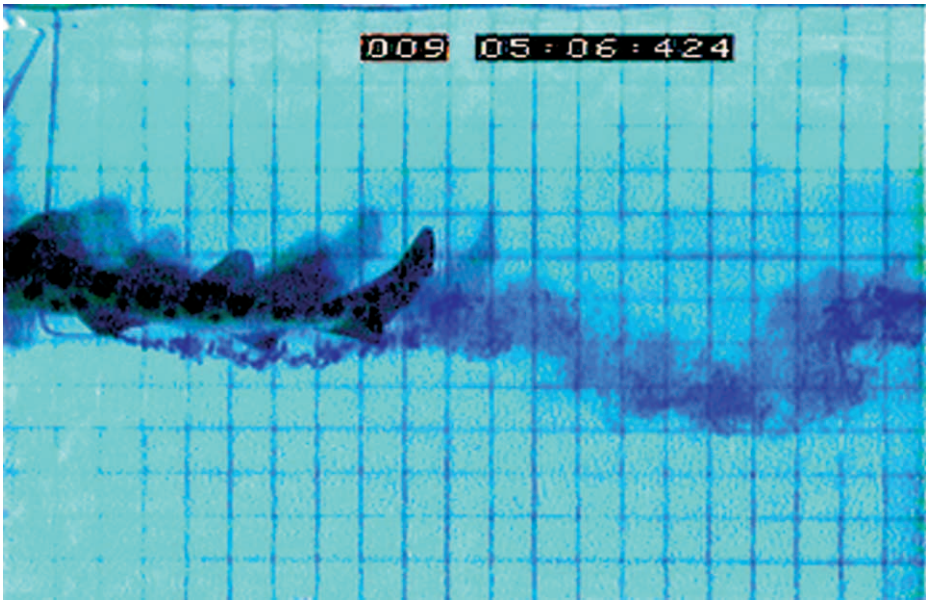

Fig. 12. Dye injected behind the paired fins and lateral to a swimming leopard shark. The tail has just passed through the dye stream, deflecting it downwards. Dye deflection occurs posterior to the tail owing to the water flow in the tank past the swimming shark, which is holding position in the earth frame of reference. Note that there are two separate shadows on the back wall of the chamber from the two light sources shining on the shark's tail; these should not be confused with the dye stream moving posteriorly to the shark. Each square in the grid behind the shark is 2 cm wide, the shark is 37 cm in total length L and is swimming at $1.2\,L\,s^{-1}$.

in the beat when the dorsal vertices of triangle G (points 7 and 4) have moved laterally relative to point 5 does triangle G orientation pass through an angle of 90° to the *xz* plane and become acute with respect to the horizontal. However, even at this time, the acute orientation of triangle G is coupled with an obtuse orientation in other triangles so that the overall tail would still be predicted to impart a negative *y* component to water movement (Fig. 9; time C). Finally, the times during which the ventral lobe is inclined at an acute angle occur when the velocity of that surface is relatively low. Hence, the contribution to thrust of triangle G, at an acute orientation is likely to be low.

Comparative and experimental issues

Although we have described heterocercal tail kinematics in the leopard shark, there are no detailed kinematic data on the caudal fin of other sharks. Does the heterocercal tail function according to the classical model for all sharks? We suspect not, as many species possess tails that could be considered to be nearly homocercal in shape (i.e. lamnid species; see Thomson and Simanek, 1977; Reif and Weishampel, 1986). Certainly the size of the terminal lobe relative to the ventral lobe and the stiffness of the tail and its lobes will play a major role in determining how out of phase the terminal and ventral lobes are with respect to one another during the tail beat. Conversely, many deep-living sharks possess markedly heterocercal tails and yet have lipid-dense livers that are thought to function in providing buoyancy. The role of the larger terminal lobe in locomotion in such sharks is unexplored, as is the direction of force produced during the tail beat.

Although we have presented data on the heterocercal tail in one species of elasmobranch, many other fishes also possess tails with a heterocercal shape. Does the heterocercal tail in primitive ray-finned fishes, such as sturgeon or paddlefish, function according to the classical model of heterocercal tail function? The taxonomic diversity of fish taxa with heterocercal tail shapes suggests that we may find unexpected diversity of function once three-dimensional kinematic data are obtained from a broad array of species.

Even with the analysis of three-dimensional kinematics of specific regions of the tail and a consequent better understanding of heterocercal tail function, our study has a number of limitations which need to be addressed in future work. First, we did not directly measure force production by the heterocercal tail. Morphological and kinematic data can contribute greatly to an understanding of locomotor hydrodynamics and allow general inferences about thrust (as seen in work on insect locomotion; e.g. Ellington, 1984*a*,*b*). However, given the complexities of tail movement described here, it is unlikely that thrust production by the heterocercal tail will be understood completely until more complete flow visualization studies are undertaken to map the flow field around the tail. Our calculations of triangle planar angles and movement vectors serve only as a visualization of tail motion, not as a direct indication of force or water movement. Tail morphology is not equivalent to simple triangular surfaces, nor are the movement patterns steady state. Furthermore, it is reasonable to assume that the beating tail generates a wake with a complex structure. Our inability to predict where eddies and turbulence might be formed by the morphologically asymmetrical trailing edge of the tail leaves us still with a simplistic understanding of heterocercal tail function.

We have not yet investigated the effects of speed on tail kinematics. While our qualitative observations of leopard sharks swimming at speeds of up to $2\,L\,s^{-1}$ suggest that the basic kinematic patterns described here also hold at higher speeds, many details of tail function may change with increasing speed. In addition, it has been suggested that the relative position of the terminal lobe may be adjusted by the shark, using intrinsic tail muscles. The question of whether sharks can actively control the angle of the heterocercal tail as a whole or actively alter the motion of specific tail lobes and

thus adjust the force balance on the body has yet to be addressed with quantitative kinematic data.

Thanks are owed to several facilities for supplying leopard sharks: California Department of Fish and Game/Doheny State Park, Saddleback College, Orange Coast Aquarium, University of California Santa Barbara, and S. Anderson, California State University Long Beach, and M. Martinez, and California Marine Specialties. Our appreciation also to A. Gibb, G. Gillis, E. Schmidt, M. Ashley-Ross, P. Webb, B. Jayne, B. Clark and two anonymous referees for helpful comments on this study and/or on the manuscript. This work was supported by NSF grant IBN9507101 to G.V.L.

References

AFFLECK, R. J. (1950). Some points in the function, development and evolution of the tail in fishes. *Proc. Zool. Soc., Lond.* **120**, 349–368.

ALEEV, Y. G. (1969). *Function and Gross Morphology in Fish*, translated from the Russian by M. Raveh. Jerusalem: Keter Press.

ALEXANDER, R. MCN. (1965). The lift produced by the heterocercal tails of Selachii. *J. exp. Biol.* **43**, 131–138.

BAINBRIDGE, R. (1963). Caudal fin and body movements in the propulsion of some fish. *J. exp. Biol.* **40**, 23–56.

BLAKE, R. W. (1983). *Fish Locomotion*. Cambridge: Cambridge University Press.

CARROLL, R. L. (1988). *Vertebrate Paleontology and Evolution*. San Francisco: W. H. Freeman and Co.

ELLINGTON, C. P. (1984*a*). The aerodynamics of hovering insect flight. II. Kinematics. *Phil. Trans. R. Soc. Lond. B* **305**, 41–78.

ELLINGTON, C. P. (1984*b*). The aerodynamics of hovering insect flight. II. Morphological parameters. *Phil. Trans. R. Soc. Lond. B* **305**, 17–40.

GOSLINE, W. A. (1971). *Functional Morphology and Classification of Teleostean Fishes*. Honolulu: University of Hawaii Press.

GROVE, A. J. AND NEWELL, G. E. (1936). A mechanical investigation into the effectual action of the caudal fin of some aquatic chordates. *Annls Mag. nat. Hist.* **17**, 280–290.

HOPSON, J. A. (1974). The functional significance of the hypocercal tail and lateral fin fold of anaspid ostracoderms. *Fieldiana Geol.* **33**, 83–93.

JAYNE, B. C. AND LAUDER, G. V. (1994). How swimming fish use slow and fast muscle fibers: implications for models of vertebrate muscle recruitment. *J. comp. Physiol.* A **175**, 123–131.

JAYNE, B. C. AND LAUDER, G. V. (1995). Are muscle fibers within fish myotomes activated synchronously? Patterns of recruitment within deep myomeric musculature during swimming in largemouth bass. *J. exp. Biol.* **198**, 805–815.

KEITHAN, E. D., MA, J. Y. AND RASCHI, W. (1992). Tendon structure of the caudal fin in the blue shark, *Prionace glauca*. *Aust. J. mar. fresh. Res.* **43**, 149–156.

LAUDER, G. V. (1989). Caudal fin locomotion in ray-finned fishes: historical and functional analyses. *Am. Zool.* **29**, 85–102.

MCFARLAND, W. N., POUGH, F. H., CADE, T. J. AND HEISER, J. B. (1979). *Vertebrate Life*. New York: Macmillan Publ. Co., Inc.

MCGOWAN, C. (1991). *Dinosaurs, Spitfires and Sea Dragons*. Cambridge: Harvard University Press.

OLSON, E. C. (1971). *Vertebrate Paleozoology*. New York: John Wiley.

REIF, W.-E. AND WEISHAMPEL, D. B. (1986). Anatomy and mechanics of the lunate tail in lamnid sharks. *Zool. Jb. Anat.* **114**, 221–234.

SIMONS, J. R. (1970). The direction of the thrust produced by the heterocercal tails of two dissimilar elasmobranchs: the Port Jackson shark, *Heterodontus portusjacksoni* (Meyer) and the piked dogfish, *Squalus megalops* (Macleay). *J. exp. Biol.* **52**, 95–107.

THOMSON, K. S. (1976). On the heterocercal tail in sharks. *Paleobiol.* **2**, 19–38.

THOMSON, K. S. (1990). The shape of a shark's tail. *Am. Sci.* **78**, 499–501.

THOMSON, K. S. AND SIMANEK, D. E. (1977). Body form and locomotion in sharks. *Am. Zool.* **17**, 343–354.

VIDELER, J. J. (1975). On the interrelationships between morphology and movement in the tail of the cichlid fish *Tilapia nilotica* (L.). *Neth. J. Zool.* **25**, 143–194.

VIDELER, J. J. (1993). *Fish Swimming*. New York: Chapman & Hall.

VOGEL, S. (1981). *Life in Moving Fluids: the Physical Biology of Flow*. Boston: Willard Grant Press.

WEBB, P. W. (1973). Effects of partial caudal-fin amputation on the kinematics and metabolic rate of underyearling sockeye salmon (*Oncorhynchus nerka*) at steady swimming speeds. *J. exp. Biol.* **59**, 565–581.

WEBB, P. W. (1975). Hydrodynamics and energetics of fish propulsion. *Bull. Fish. Res. Bd Can.* **190**, 1–159.

WEBB, P. W. (1993). The effect of solid and porous channel walls on steady swimming of steelhead trout *Oncorhynchus mykiss*. *J. exp. Biol.* **178**, 97–108.

WEBB, P. W. AND SMITH, G. R. (1980). Function of the caudal fin in early fishes. *Copeia* **1980**, 559–562.

WILSON, M. V. H. AND SOEHN, K. L. (1990). Discovery of complete silurian fish – oldest heterostracan tail has dermal fin rays. *Naturwissenschaften* **77**, 328–330.

ZAR, J. H. (1984). *Biostatistical Analysis*. Englewood Cliffs: Prentice-Hall, Inc.